JOURNAL OF GEOPHYSICAL RESEARCH, VOL. 111, D24202, doi:10.1029/2006JD007145, 2006

Characterization of atmospheric aerosols at Monte Cimone, Italy, during summer 2004: Source apportionment and transport mechanisms

F. Marenco,[1] P. Bonasoni,[2] F. Calzolari,[2] M. Ceriani,[3] M. Chiari,[4] P. Cristofanelli,[2] A. D'Alessandro,[1] P. Fermo,[5] F. Lucarelli,[4] F. Mazzei,[1] S. Nava,[4] A. Piazzalunga,[5] P. Prati,[1] G. Valli,[3] and R. Vecchi[3]

Received 1 February 2006; revised 17 July 2006; accepted 27 July 2006; published 16 December 2006.

[1] Atmospheric aerosols in the PM_{10} and PM_1 fractions have been sampled at the Global Atmospheric Watch station Mount Cimone, Italy (2165 m above mean sea level) for 3 months during summer 2004, and simultaneous size distributions have been derived by means of an optical particle counter. Samples have been analyzed by X-ray fluorescence, ion chromatography, and thermal-optical methodology in order to quantify their elemental, ionic, and carbonaceous constituents. The concentration of PM_{10} was 16.1 ± 9.8 $\mu g\ m^{-3}$ (average and standard deviation). Source apportionment allowed us to identify, quantify and characterize the following aerosol classes: anthropogenic pollution (10 $\mu g\ m^{-3}$), mineral dust (4 $\mu g\ m^{-3}$), and sea salt (0.2 $\mu g\ m^{-3}$). Pollution has been further split into ammonium sulfate (44%), organic matter (42%), and other compounds (14%). The nitrate/sulfate ratio in the polluted aerosol was 0.1. Fine particles have been completely related to the polluted aerosol component, and they represented 70% in weight of pollution. Coarse particles characterized the dust and salt components, and crustal oxides have been found to be the largest responsible for the aerosol concentration variations that occurred during the campaign. Nitrate has also been found in the coarse particles, representing ~10% of mineral dust. The analysis of the transport mechanisms responsible for aerosol fluctuations permitted us to identify the origin of the major aerosol components: Pollution has been ascribed to regional transport driven by boundary layer meteorology, whereas mineral dust has been related to long-range transport events originating in the Sahara and Sahel. A particularly significant Saharan episode has been identified on 10 August 2004 (PM_{10} daily concentration, 69.9 $\mu g\ m^{-3}$). Average elemental ratios for the African dust events were as follows: Si/Al = 2.31, Fe/Ca = 0.94, Ca/Al = 0.90, K/Ca = 0.44, Ti/Ca = 0.11, and Ti/Fe = 0.12.

Citation: Marenco, F., et al. (2006), Characterization of atmospheric aerosols at Monte Cimone, Italy, during summer 2004: Source apportionment and transport mechanisms, *J. Geophys. Res.*, *111*, D24202, doi:10.1029/2006JD007145.

1. Introduction

[2] Atmospheric aerosols are a major unknown to climate research since they present a large day-to-day variability in terms of origin, composition, size distribution and global distribution. A major issue concerns the magnitude of the natural and anthropogenic components of the aerosol population [*Intergovernmental Panel on Climate Change*, 2001]. Besides being important for the evaluation of climatic impacts, the same issue is relevant to the application of environmental limits on aerosol concentration. In fact, local and regional sources are not the only factor affecting the aerosol contribution at a measurement site, since long-range transport can occur. The Sahara desert, for instance, is a major source of particulate matter, usually considered of natural origin (although a relevant part of mineral aerosols is attributed to desertification and land misuse, and thus to human activities [*Tegen and Fung*, 1995]). Saharan dust can travel over distances of several thousands kilometers [*Morales*, 1986; *Chiapello et al.*, 1999; *Borbély-Kiss et al.*, 2004], reaching altitudes going almost up to the tropopause [*Gobbi et al.*, 2000]. In southern European environments Saharan sources may cause a number of PM_{10} exceedances with respect to air quality standards [*Rodríguez et al.*, 2001].

[1] Physics Department, University of Genoa and Istituto Nazionale di Fisica Nucleare-Genova, Genoa, Italy.
[2] Institute of Atmospheric Sciences and Climate, National Research Council, Bologna, Italy.
[3] General Applied Physics Institute, University of Milan and Istituto Nazionale di Fisica Nucleare-Milano, Milan, Italy.
[4] Physics Department, University of Florence and Istituto Nazionale di Fisica Nucleare-Firenze, Florence, Italy.
[5] Inorganic, Metallorganic and Analytical Chemistry Department, University of Milan, Milan, Italy.

0148-0227/06/2006JD007145$09.00

[3] Aerosol samples are usually collected at urban sites. However, as local sources dominate in cities, it can be difficult to isolate features proper of long-range transport and of background conditions. Instead, sampling at remote sites is mostly useful for characterizing the regional background and for identifying air mass transport effects [see, e.g., *Braga Marcazzan et al.*, 1993; *Schwikowski et al.*, 1995]. Aerosol sources can be revealed through the evaluation of the composition. More insight is given by source apportionment and the correlation with relevant meteorological parameters.

[4] In this work, results of aerosol samplings in the PM_{10} and PM_1 fractions carried out in 2004 at the Mount Cimone Global Atmospheric Watch (GAW) station during a 3-month summertime campaign are presented. Mount Cimone (44°11′N, 10°42′E, 2165 m above mean sea level (amsl)), the highest peak of the Italian northern Apennines, is considered representative of southern European continental background conditions [*Bonasoni et al.*, 2000b; *Fischer et al.*, 2003]. Located in the free troposphere most of the time, it has, however, been verified that during the warm season boundary layer air masses may reach this site, because of vertical mixing and mountain wind regime [*Fischer et al.*, 2003; *Van Dingenen et al.*, 2005].

[5] The aerosol sampling campaign started on 30 June (Julian day (JD) 182) and ended on 6 October 2004 (JD 280), with the aim of improving the description of the background aerosols in southern Europe, with emphasis on fine particles, and on evaluating the contribution of remote and regional sources. A significant subset of aerosol properties (size-fractionated concentration, detailed composition and size distribution) have been continuously monitored. In the past, the compositional characterization of aerosol samples collected at this mountain site has been examined for ionic, carbonaceous and refractory components [*Putaud et al.*, 2004; *Van Dingenen et al.*, 2005]. Within this research, elemental analysis has allowed us to identify the major aerosol components, in order to obtain a more complete picture.

[6] For the size fraction PM_1, only few previous elemental characterizations at mountain sites have been reported before [*Streit et al.*, 2000]. The study of this fraction is of importance since accumulation mode particles (0.1–1 μm diameter) dominate radiative effects in the visible range, due to the fact that they are preponderant in number and, having a size comparable to visible wavelength, they have a large scattering efficiency. Moreover, it is in the fine aerosol fraction that the anthropogenic influence is preponderant, including emissions of strongly absorbing aerosols such as black carbon.

[7] Aerosol composition and air mass origin are intimately correlated and can be used to distinguish between aerosol types and thus quantify the natural and anthropogenic components. In this paper, source apportionment techniques are used for the characterization of the aerosols, and the description of the relevant meteorological drivers is attempted using back trajectories and Planetary Boundary Layer data.

2. Sampling and Methods

2.1. Field Campaign

[8] Aerosols have been sampled on 47 mm diameter filters, using CEN-equivalent sequential samplers from TCR-Tecora equipped with PM_{10} and PM_1 sampling heads. PM_{10} was sampled on polytetrafluoroethylene (PTFE) substrate, at the rate of one filter every 24 hours. PM_1 was sampled in parallel on both PTFE and prefired quartz fiber filters, at the rate of one every 48 hours. Sampling was performed at a constant air flux of 2.3 $m^3\ h^{-1}$ (actual flux) through each filter, and filter changes were programmed to take place at midnight local time.

[9] PM_{10} sampling on PTFE started on JD 182; PM_1 sampling on PTFE started on JD 191; and PM_1 sampling on quartz fiber started on JD 213. All samplings ended on JD 280, after a 99-day-long campaign. Because of adverse meteorological conditions, several data have been lost: Finally, 57/99 PTFE-PM_{10} samples, 24/44 PTFE-PM_1 samples, and 21/34 quartz-fiber-PM_1 samples have been retained. Data loss has occurred between JD 197 and 210 and after JD 254, simultaneously on the three samplers.

[10] Additional daily PM_{10} samples on PTFE filters have been collected from JD 206 to 277 in Modena, Italy, by the Regional Agency for Prevention and Environment, Emilia-Romagna [*D'Alessandro et al.*, 2006]. Modena is a middle-sized town located in the Po Valley (60 km north of Mount Cimone, 30 m amsl). These samples are used here as a term of comparison with the Mount Cimone results, in order to give a hint on the correlation between the two sites and on transport phenomena.

[11] In addition to samplers, a Grimm 1.108 optical particle counter (OPC) placed at Mount Cimone provided the aerosol number size distribution for diameters (D_p) between 0.3 and 20 μm in 15 size channels, with a 1-min time resolution. The instrument is based on the quantification of the 90° scattering of light by aerosol particles. According to the specifications, the reproducibility of the OPC in particle counting is ±2% [*Putaud et al.*, 2004]. Hereinafter, when referring to the OPC measurements, we use the term "fine particles" to denote particles with 0.3 $\mu m < D_p \leq 1\ \mu m$, and the term "coarse particles" for $1\ \mu m < D_p \leq 20\ \mu m$.

2.2. Laboratory Analyses

[12] Samples have been analyzed gravimetrically after being conditioned for 48 hours at constant temperature (20 ± 1°C) and relative humidity (50 ± 5%). To determine the particulate matter concentration, filters have been weighed both before and after sampling with an analytical balance (sensitivity 1 μg). All concentrations given in this paper, gravimetric and compositional, refer to normalized air volumes, i.e., to 1 atm and 0°C.

[13] Information on the aerosol composition has been gathered through the use of energy dispersive X-ray fluorescence (ED-XRF). This technique has sensibility for elements with atomic number $Z \geq 11$, and thus the carbonaceous part and nitrates remain undetected [*Van Grieken and Markowicz*, 1993]. The technique is efficient in distinguishing several important aerosol types, such as for instance mineral dust, sulfur-containing particles and sea salt. Elemental concentrations on the PTFE filters were determined at the laboratories of the Universities of Genova and Milano, using two ED2000 spectrometers by Oxford Instruments, following a methodology already adopted in previous works [*Marcazzan et al.*, 2001]. The following elements have been identified: Na, Mg, Al, Si, P, S, Cl, K, Ca, Ti, V, Cr, Mn, Fe, Ni, Cu, Zn, Se, Br, Sr, Pb. Detection limits were 2–100 ng cm^{-2} on the filter deposit (depending on element);

in terms of airborne concentration, 0.6–30 ng m^{-3} for 24-hour samples and 0.3–15 ng m^{-3} for 48-hour samples.

[14] The water-soluble inorganic portion of the Mount Cimone PTFE samples has been determined by standard ion chromatography, IC [*Chow and Watson*, 1999], using an ICS-1000 Ion Chromatography System (Dionex). A quarter of each filter has been extracted in Milli-Q water: Three successive extractions of 20 min in an ultrasonic bath were needed for a nearly complete recovery, with the renewal of the water at each step. In each of the 3 extraction steps 2 mL of Milli-Q water have been used. For each of the three solutions obtained, an aliquot of 1.5 mL was drawn and the three aliquots joined in a clean tube from which the solution for ions determination (100 μL) was withdrawn. The extracts have been analyzed by IC for major ionic species with an estimated overall uncertainty of 10–15% or better on ionic concentrations. Anions determination has been performed by means of a Ion Pac AS14A column (Dionex) using 8 mM Na_2CO_3/1 M $NaHCO_3$ as eluent at 1 mL min^{-1} flow rate and, for the detection, a conductivity system equipped with a ASRS-ULTRA suppression mode (Dionex). Cations determination has been performed by means of a CS12A column (Dionex) using 20 mM methanesulfonic acid as eluent at 1 mL min^{-1} flow rate and, for the detection, a conductivity system equipped with a CSRS-ULTRA suppression mode (Dionex). The concentration of the following species has been retained: ammonium (NH_4^+), sulfate (SO_4^{2-}) and nitrate (NO_3^-).

[15] The carbonaceous content of samples deposited on Mount Cimone PM_1 quartz fiber filters has been quantified for both organic (OC) and elemental carbon (EC). A rectangular portion (area 1.5 cm^2) of each filter has been analyzed by a thermal-optical transmission method (TOT) by means of an OC/EC carbon analyzer (Sunset Laboratory Inc., USA) using the NIOSH 5040 protocol [*Chow et al.*, 2001]. Filters were prefired prior to sampling, by heating them at 700°C for 1 hour. Details on the methodology are given by *Birch and Cary* [1996]. The estimated uncertainty on derived concentrations is 5–10%.

2.3. Source Apportionment Methodologies

2.3.1. Aerosol Composition

[16] Estimate of mineral dust concentration has been made by combining the concentrations for crustal elements, multiplied by the respective molar correction factors, according to *Eldred et al.* [1987] and *Malm et al.* [1994]. The factors have been derived assuming that the elements are present in the form of oxides, according to the composition of the Earth's crust given by *Lide* [1992]; the two iron oxides have been assumed equally abundant; and the concentration of K has been extrapolated from Fe so that nonsoil K (from smoke) is not accounted (based on our correlation line between the two elements, $[K]_{soil} = 0.47\ [Fe]$). Finally, molar correction factors have been proportionally increased by 12% to account other compounds present in the average sediment. The relationship used is the following:

$$\begin{aligned}[\text{crustal oxides}] &= 1.12 \times \{1.658[Mg] + 1.889[Al] + 2.139[Si] \\ &\quad + 1.399[Ca] + 1.668[Ti] + 1.582[Mn] \\ &\quad + (0.5 \times 1.286 + 0.5 \times 1.429 + 0.47 \times 1.204)[Fe]\}.\end{aligned}$$

The above formula yields correct results for all types of soil listed by *Lide* [1992], except for limestone where a large fraction of the mass, given by carbonate, is missed.

[17] A first estimate of sea salt could be given by [Na] +[Cl]; however, actual sea salt resembles more a mixture of NaCl (82% by weight), $MgCl_2$ (8%) and $MgSO_4$ (10%). A full characterization is given by *Lide* [1992], and based on the composition of seawater given therein the following relationship has been adopted:

$$[\text{sea salt}] = 1.46[Na] + [Cl]$$

which is similar to the approach by *Virkkula et al.* [1999]. The 1.46 factor in front of Na stands for other ionic constituents (representing 14% of sea salt), and Cl is added separately. It has to be noted, however, that a different approach is possible [*Malm et al.*, 1994]: Sea salt can be calculated from Na only, using the appropriate molar correction factor. The latter approach often results in a larger estimate, since in aerosols Na and Cl are seldom found in the same proportion as in seawater: Cl can be volatilized by reacting with acidic species [*Seinfeld and Pandis*, 1998; *Lee et al.*, 1999] or with ammonium nitrate on the samples [*Querol et al.*, 2001]. With our approach, we determine how much sea salt is present in the samples when they are weighed and irradiated, which is what is mostly useful for mass reconstruction. By estimating sea salt from Na only, instead, one tries to determine how much of this compound could have been present in the air mass at its origin. It also has to be mentioned that Na concentration might be underestimated because of self-attenuation within the sample during ED-XRF irradiation [see, e.g., *D'Alessandro et al.*, 2003]. By assuming attenuation coefficients given by J. H. Hubbell and S. M. Seltzer (Tables of X-ray attenuation coefficients and mass energy-absorption coefficients, http://physics.nist.gov/PhysRefData/XrayMassCoef/cover.html, National Institute of Standards and Technology, Gaithersburg, Maryland, 1996) and a composition of pure NaCl, this underestimation has been evaluated to amount to as much as 35% for 2 μm diameter particles (close to the effective diameter for sea salt particles that we have found; see section 3.4). No correction has, however, been performed in this work, as the actual composition of sea salt particles within the samples is unknown.

[18] Concerning sulfur compounds, a few preliminary considerations based on our IC results must be made, based on the observation that daily S, SO_4^{2-} and NH_4^+ concentrations have been found to be strongly correlated. The correlation coefficient between S and SO_4^{2-}, obtained by linear regression, is 0.98 for the PM_{10} data and 0.995 for PM_1; the correlation coefficient between NH_4^+ and SO_4^{2-} is 0.97 for PM_{10} (after the removal of three outliers) and 0.98 for PM_1. The overall average SO_4^{2-}/S ratio (PM_{10} and PM_1 samples together) is 3.4 ± 0.4, which is compatible with the hypothesis that all S is present as sulfate ion (the value expected for sulfate is 3.00). The overall average SO_4^{2-}/NH_4^+ ratio (PM_{10} and PM_1 samples together) is 2.4 ± 0.3, and is compatible with the assumption that all sulfate is neutralized by ammonium, in the form of ammonium sulfate, $(NH_4)_2SO_4$ (the expected ratio for pure ammonium sulfate is 2.66). The data are therefore compatible with associating S to secondary sulfates, originating from sulfur dioxide due

to fossil fuel burning, and transported from polluted areas (as also assumed by *Malm et al.* [1994]). Ammonium sulfate has been quantified in two ways, multiplying the concentration of elemental S by 4.125 and multiplying the concentration of sulfate ion by 1.375; in the following, we have considered the average between these two determinations. Their difference is compatible within the experimental uncertainties (±5–10% on XRF concentrations, ±10–15% on determinations by IC). It has to be mentioned that the second concentration exceeds the first one by 10–12% (systematic): This may be explained by the fact that the techniques were independently calibrated.

[19] Nitrate deserves similar observations as those made for sulfate. One must, however, be aware of the fact that NO_3^- measurements are affected by sampling artifacts, since losses may take place in the form of gaseous HNO_3, and moreover NH_4^+ associated with nitrate may evaporate during sampling [*Henning et al.*, 2003]. In this paper, ammonium nitrate has been evaluated by adding together the excess NH_4^+, determined after substraction of the quantity needed to neutralize SO_4^{2-}, and the corresponding equivalents of NO_3^-. The remaining part of NO_3^- has been separately accounted as unbalanced nitrate: In the sample the ionic balance might have been provided by H^+ (acidic aerosols), or the metals observed by ED-XRF (and already accounted as crustal oxides). It is known, for instance, that mineral dust particles containing calcium carbonates (calcite and dolomite) may react with gaseous nitric acid in the atmosphere to form nitrate salts, and that this reaction is not surface-limited and affects the bulk of the particle [*Krueger et al.*, 2004]. Considering NH_4^+, SO_4^{2-} and NO_3^-, in our data set the balance between anions and cations is verified in the PM_1 fraction, but not for PM_{10} where an excess anions is found, denoting the presence of unbalanced NO_3^-.

[20] Organic matter (OM) can be deduced from OC with a conversion coefficient of 2, appropriate for rural sites as documented by *Turpin and Lim* [2001] and *El-Zanan et al.* [2005]. The use of a "large" OM/OC ratio for rural sites is explained by the fact that, on one side the contribution of biogenic aerosols is expected larger than in urban areas, and on the other side anthropogenic particles tend to be aged and therefore more oxygenated [*El-Zanan et al.*, 2005]. It must be remembered, however, that using an a priori ratio is not a robust approach, as the mix of organic compounds in aerosols varies [*Turpin and Lim*, 2001].

2.3.2. Principal Components

[21] The correlation of multiple variables can be studied by means of multivariate statistical techniques [*Mather*, 1976; *Hansson et al.*, 1984; *Swietlicki et al.*, 1987; *Marcazzan et al.*, 2003]. Here principal component analysis (PCA) has been applied to the aerosol data set: The resulting factor loadings table is used to group measured variables into different components, each representing a set exhibiting a correlated behavior. The fluctuation of elemental concentrations within each component can therefore be assumed to be associated to a common cause, e.g., a same production or advection mechanism. Moreover, absolute principal component analysis (APCA) permits to quantify the portion of the measured aerosol concentration, determined gravimetrically, that is associated to each identified component [*Thurston and Spengler*, 1985; *Keiding et al.*, 1986; *Swietlicki et al.*, 1996]. On the basis of a statistical approach, the method is thus capable of quantifying the overall portion of the aerosol concentration associated to each component, including the part that is not directly observed by our analytical techniques: For instance, the ED-XRF data set does not include light elements such as H, C, N and O; however, the APCA may reconstruct the overall concentration in each component.

[22] PCA has been applied to the PM_{10} data set only, since the number of PM_1 samples has been judged statistically insufficient; moreover, as will be shown, source apportionment for PM_1 appears quite simple so as to be interpreted directly.

2.4. Meteorological Interpretation Tools

[23] Air masses reaching Mount Cimone have been traced using back trajectories computed using the Hybrid Single-Particle Lagrangian Integrated Trajectory (Hysplit) model (R. R. Draxler and G. D. Rolph, NOAA ARL HYSPLIT model, http://www.arl.noaa.gov/ready/hysplit4.html, NOAA Air Resources Laboratory, Silver Spring, Maryland, 2003), initialized with synoptic meteorological fields produced by the National Centers for Environmental Prediction and archived at the NOAA Air Resources Laboratory (FNL archive). A critical review on the use of trajectories is given by *Stohl* [1998], and the advice therein has been found precious for this research, with particular reference to the sources of error and divergence and the recommendation on using trajectory ensembles. The latter recommendation is also supported by the work of *Seibert* [1993] and *Baumann and Stohl* [1997].

[24] For each campaign day we have also determined the daytime mixing height, or mixed layer depth, from radiosondes launched at San Pietro Capofiume (100 km northeast of Mount Cimone, 38 m amsl) at 1400 local time; the radiosonde data having been downloaded from the University of Wyoming Web site http://weather.uwyo.edu/upperair/sounding.html). For each profile, the mixing height has been set by looking at discontinuities in the gradient of potential temperature, absolute humidity, and wind speed and direction. Although set in a subjective manner, we estimate ambiguities in the mixing height determination not being larger that a few hundred meters. San Pietro Capofiume represents the nearest radiosounding station in respect with Mount Cimone, and data from this station have been used in a wide number of research projects and publications for deriving the vertical characterization of the atmosphere over the Po basin and explaining the behavior of atmospheric constituents at Mount Cimone [e.g., *Bonasoni et al.*, 2000a; *Seibert et al.*, 2000; *Cristofanelli et al.*, 2006]. Because of the flat orography of the Po Valley, soundings carried out at San Pietro Capofiume can be considered representative of a large geographical area lying between the Apennines and the eastern coast of Emilia-Romagna. Obviously, some differences in the mixing height are possible; nevertheless the weather conditions promoting the increase of mixed layer depth, such as intense solar radiation, large temperature and high pressure, also favor the transport of

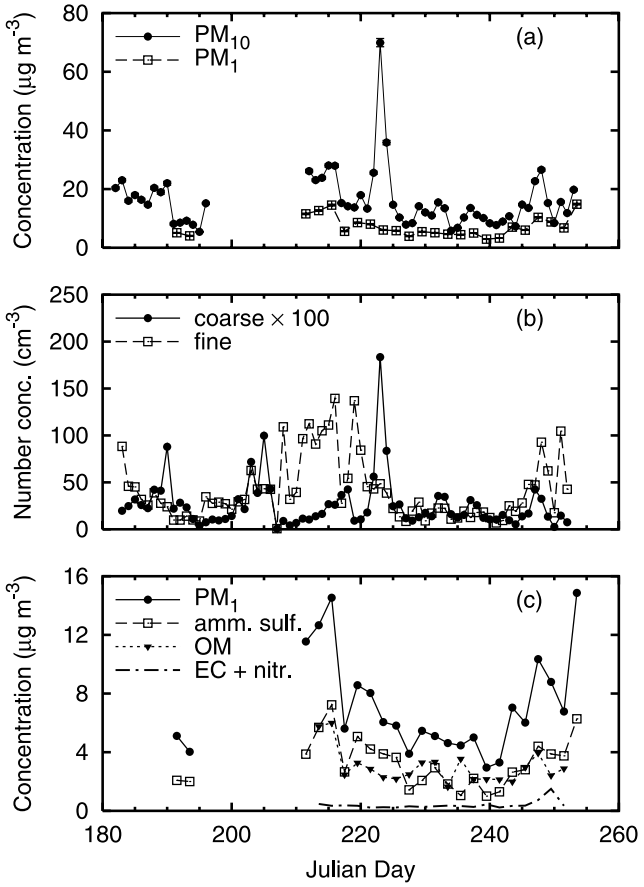

Figure 1. (a) Aerosol concentration versus time at Mount Cimone during summer 2004, based on 24-hour PM_{10} samples (solid circles, solid line) and 48-hour PM_1 samples (open squares, dashed line). (b) Particle number concentration, daily averages for coarse (solid circles, solid line) and fine (open squares, dashed line) particles. Data for the coarse mode are multiplied by 100 for graphical purposes. (c) PM_1 concentration (solid circles, solid line) at Mount Cimone during summer 2004, decomposed into ammonium sulfate (open squares, dashed line), organic matter (solid triangles, dotted line), and EC plus nitrate (dashed-dotted line).

pollution from lowlands to the northern Apennines [*Seibert et al.*, 2000; *Bonasoni and Cristofanelli*, 2001].

3. Campaign Results

3.1. General Features of Mount Cimone Aerosols

[25] In Figures 1a and 1b, the graphs of the PM_{10} and PM_1 aerosol concentration (determined gravimetrically) and of the particle number concentration for coarse and fine particles (determined by OPC) are displayed. The following average quantities have been determined: PM_{10} 16.1 $\mu g\ m^{-3}$ (standard deviation 9.8 $\mu g\ m^{-3}$); PM_1 7.1 $\mu g\ m^{-3}$ (standard deviation 3.4 $\mu g\ m^{-3}$); coarse particles 0.26 cm^{-3} (standard deviation 0.34 cm^{-3}); and fine particles 40 cm^{-3} (standard deviation 40 cm^{-3}); where the standard deviation is a measure of the variability of the observed variable.

[26] These quantities show large variations. As far as PM_{10} is concerned, for instance, the minimum and maximum concentrations amount to 5.4 and 69.9 $\mu g\ m^{-3}$, respectively. The most striking feature is the aerosol peak on days 222–224; by removing those three days from the data set, the PM_{10} average reduces to 14.5 $\mu g\ m^{-3}$ (standard deviation: 6.0 $\mu g\ m^{-3}$). The PM_1 concentration seems unaffected by the large PM_{10} variations that occur on JD 222–224 (Figure 1a): This indicates that the observed feature has to be ascribed to coarse particles, as confirmed by the OPC data (Figure 1b).

[27] Tables 1 and 2 display the average concentrations of individual constituents, together with the standard deviations over the campaign period, medians, low and high percentiles. Among detected elements, the most abundant one is S, with a concentration of 1.0 $\mu g\ m^{-3}$ in PM_{10} and 0.7 $\mu g\ m^{-3}$ in PM_1; its largest part (70%) is thus in the fine fraction. Other elements abundant in the PM_{10} fraction (but not in PM_1) are Si, Ca, Al, Fe, Na, K, Mg, Cl and Ti. Traces of P, V, Mn, Ni, Cu, Zn, Br, Sr and Pb have also been found (average values in $PM_{10} \leq 10\ ng\ m^{-3}$ for each of them). Noteworthy are also the concentrations of SO_4^{2-} (3.5 $\mu g\ m^{-3}$ in PM_{10} and 2.4 $\mu g\ m^{-3}$ in PM_1) and NH_4^+ (1.4 $\mu g\ m^{-3}$ in PM_{10} and 1 $\mu g\ m^{-3}$ in PM_1): Their distribution among PM_1 and PM_{10} reflects that of S (70–72% in PM_1), confirming the ammonium sulfate assumption. Relevant are also the amounts of OC in PM_1, 1.5 $\mu g\ m^{-3}$, and NO_3^- in PM_{10}, 0.8 $\mu g\ m^{-3}$.

3.2. Characterization of PM_1 at Mount Cimone

[28] From Table 2 and the above considerations, we deduce that one of the principal constituents of PM_1 is ammonium sulfate, with an average concentration of 3.1 $\mu g\ m^{-3}$. OC is also significant, with 1.5 $\mu g\ m^{-3}$ on average, corresponding to 3.0 $\mu g\ m^{-3}$ organic matter. The reconstruction of the PM_1 aerosol is detailed in Table 3 and Figure 1c. Besides the two major components mentioned above, minor constituents have been identified as ammonium nitrate, EC and crustal oxides (0.6 $\mu g\ m^{-3}$ globally). Finally, one ends up with a reconstructed mass of 6.7 $\mu g\ m^{-3}$, representing 94% of the gravimetric datum (7.1 $\mu g\ m^{-3}$). The two major contributors, ammonium sulfate and organic matter, are found in a nearly 1:1 proportion. Both are individually very well correlated to PM_1 (linear regression correlation coefficients of 0.94 and 0.81, respectively): We can thus reasonably assume that during the campaign PM_1 is the result of a relatively constant mix of these two aerosol types. The same cannot be said for ammonium nitrate and EC, which besides being observed in a relatively small amount, are poorly correlated to the overall PM_1 concentration.

3.3. Characterization of PM_{10} at Mount Cimone

[29] PCA has been applied to the gravimetric and elemental PM_{10} data set, where the daily size-resolved number concentrations determined by OPC have been included in the analysis: Table 4 lists the resulting factor loadings. Ionic concentrations have been omitted because ten samples could not be submitted to IC, which is destructive, since they have been kept aside for additional analyses (but in the end the latter analyses were not possible). The ten samples were selected in correspondence to significant dust episodes (see below) and thus removing them from the data set would have been a restriction that could have significantly

Table 1. Summary of Elemental and Ionic Concentrations in PM_{10} During the Mount Cimone Campaign[a]

Element	Samples	Mean	SD	Median	10th Percentile	90th Percentile
Na	57	210	150	180	42	420
Mg	57	81	82	65	25	110
Al	57	300	460	140	40	670
Si	57	700	1100	400	120	1600
P	31	10.3	6.5	8.8	3.3	15.4
S	57	1040	570	1000	340	1780
Cl	26	82	98	45	19	175
K	57	160	210	120	53	250
Ca	57	360	550	240	73	630
Ti	53	30	50	16	5	58
V	35	3.1	1.5	2.8	1.8	4.6
Mn	49	6.2	7.0	4.5	2.2	10.3
Fe	57	260	440	140	37	400
Ni	26	1.4	0.5	1.3	0.9	2.1
Cu	50	2.9	3.1	1.8	1.2	5.3
Zn	57	9.9	6.0	8.4	3.6	19.6
Br	56	3.0	1.1	3.0	1.7	4.3
Sr	40	2.7	2.8	2.1	1.1	3.7
Pb	48	3.9	2.4	3.4	1.5	7.5
NH_4^+	47	1430	800	1240	440	2560
SO_4^{2-}	47	3500	2000	3500	1100	6200
NO_{3-}	47	840	670	700	280	1310
PM_{10}	57	16100	9800	14200	7900	25800

[a]Concentrations are given in ng m^{-3}. The "Sample" column indicates number of valid samples for which there is a detectable quantity of the given element (i.e., above the minimum detection limit). SD is standard deviation. Data are omitted for elements for which the number of valid samples is less than 40% of the total number of samples.

altered the picture given by the statistical approach. We have thus preferred removing the ionic concentrations from the data set rather than excluding these particularly significant samples.

[30] Three components have been identified. Factor 1 represents 56% of the PM_{10} variability, and is correlated to Mg, Al, Si, K, Ca, Ti, V, Mn, Fe and Sr: This sequence of elements is a clear signature of mineral dust. Factor 2, correlated to S, Zn, Br and Pb, has been associated to anthropogenic pollution, where Zn, Br and Pb are quantitatively present in traces (Table 1). Factor 3, correlated to Na and Cl, has been associated to sea salt. APCA permitted to quantify the contribution of each component, as listed in Table 5. It is also interesting to note how the number concentrations in size bins, determined by OPC, fit into this picture (Table 4): Fine particles are correlated with pollution and coarse particles with mineral dust. The separation between the two components appears to be around a diameter of 0.7 μm. No significant correlation has been found for particles above 7.5 μm.

[31] The reconstruction of the PM_{10} composition has been done also with compositional (rather than statistical) considerations, as summarized in Table 5. When they are added together, elements ascribed to the Earth's crust

Table 2. Summary of Elemental, Ionic, and Carbonaceous Compound Concentrations in PM_1 During the Mount Cimone Campaign (Similar to Table 1)[a]

Element	Samples	Mean	SD	Median	10th Percentile	90th Percentile	PM_1/PM_{10}
Al	11	10.6	6.3	9.4	4.0	16.8	0.04
Si	23	25	17	21	8	47	0.06
P	10	2.6	1.4	2.2	1.3	4.7	0.27
S	24	700	360	610	300	1230	0.70
K	24	36	25	32	10	60	0.25
Ca	23	9.0	5.5	7.0	4.2	16.7	0.04
Fe	24	8.5	8.3	5.0	1.8	17.9	0.05
Zn	24	5.9	5.0	4.2	1.5	9.7	0.54
Br	23	2.1	0.7	2.1	1.3	3.1	0.69
Pb	19	2.1	1.3	1.6	1.0	3.7	0.50
NH_4^+	24	970	460	880	480	1570	0.73
SO_4^{2-}	24	2400	1200	2100	1000	4000	0.71
NO_{3-}	24	260	350	130	90	640	0.19
OC	21	1490	560	1340	1070	1970	NA
EC	21	171	61	159	102	249	NA
PM_1	24	7100	3400	5900	3900	12300	0.47

[a]Concentrations are given in ng m^{-3}. The last column displays the average PM_1/PM_{10} ratio for each displayed element or ion. Total PM_1 and elemental and ionic concentrations have been determined from PTFE filters, while OC and EC have been determined from quartz fiber filters. NA indicates not available.

Table 3. Mass Reconstruction for the PM_1 Aerosol at Mount Cimone

Aerosol Class	Average Concentration: Micrograms per Cubic Meter	Average Concentration: Percentage
Ammonium sulfate	3.1	44
Organic matter	3.0	42
Ammonium nitrate	0.3	4
Elemental carbon	0.2	3
Crustal oxides	0.1	1
Reconstructed	6.7	94
Average PM_1	7.1	100

Table 4. Factor Loadings From Principal Component Analysis on the Mount Cimone Data Set Performed on PM_{10} Gravimetric Concentration, PM_{10} Elemental Concentrations, and Particle Number Concentrations in the OPC Size Classes[a]

Variable	Factor 1 Mineral Dust	Factor 2 Pollution	Factor 3 Sea Salt
PM_{10}, gravimetric	0.84	0.51	0.02
PM_{10} elemental concentrations			
Na	−0.01	−0.31	**0.87**
Mg	**0.97**	0.00	0.18
Al	**0.99**	0.05	−0.02
Si	**0.99**	0.07	−0.02
S	0.11	**0.87**	0.15
Cl	0.23	−0.17	**0.68**
K	**0.98**	0.14	0.00
Ca	**0.95**	0.14	−0.01
Ti	**0.99**	0.08	−0.03
V	**0.66**	0.27	0.30
Mn	**0.95**	0.16	−0.08
Fe	**0.99**	0.09	−0.03
Cu	−0.04	0.28	−0.10
Zn	0.07	**0.88**	−0.14
Br	0.18	**0.63**	0.43
Sr	**0.96**	0.11	0.04
Pb	0.27	**0.76**	−0.09
Particle number concentrations			
0.3–0.4 μm	0.01	**0.95**	−0.15
0.4–0.5 μm	0.01	**0.94**	−0.16
0.5–0.65 μm	0.11	**0.95**	−0.07
0.65–0.8 μm	**0.76**	0.57	0.23
0.8–1 μm	**0.94**	0.15	0.25
1–1.6 μm	**0.94**	0.05	0.28
1.6–2 μm	**0.87**	0.07	0.43
2–3 μm	**0.98**	0.03	0.11
3–4 μm	**0.99**	0.01	0.05
4–5 μm	**0.94**	0.00	0.11
5–7.5 μm	**0.77**	−0.06	0.18
Explained variance, %	56	21	7

[a]Factor loadings larger than 0.6 are in boldface.

Table 5. Source Apportionment of the PM_{10} Aerosol at Mount Cimone Obtained With the Stoichiometric and Multivariate (APCA) Approaches[a]

Aerosol Class	Approach		
	Stoichiometric, $\mu g\ m^{-3}$	Multivariate, $\mu g\ m^{-3}$	Multivariate, %
Mineral dust			
Crustal oxides	3.7		
Unbalanced nitrate	0.4		
Total	4.1	4.3	27
Pollution			
Ammonium sulfate	4.6		
Ammonium nitrate	0.5		
OM plus EC	NA		
Total	$\geq$5.1	9.7	60
Sea salt	0.3	0.2	1
Reconstructed		14.2	88
Average PM_{10}		16.1	100

[a]See text. NA indicates not available.

amount to 1.9 $\mu g\ m^{-3}$ in PM_{10} (campaign average); computed oxides, instead, amount to 3.7 $\mu g\ m^{-3}$. The average S concentration amounts to 1.0 $\mu g\ m^{-3}$; the average SO_4^{2-} concentration amounts to 3.5 $\mu g\ m^{-3}$, and the resulting concentration for ammonium sulfate is 4.6 $\mu g\ m^{-3}$. Sea salt has been quantified in 0.3 $\mu g\ m^{-3}$ average concentration.

[32] Nitrate is found both in the fine and coarse aerosol fractions, and mostly in the latter, since its average concentration in PM_1 represents about one third of its average concentration in PM_{10}. This observation is in line with the observations made by *Henning et al.* [2003] at the Jungfraujoch and by *Putaud et al.* [2004] at Mount Cimone, which have found nitrate internally mixed with mineral dust, because of adsorption of HNO_3. In our data set, 45% NO_3^- is balanced with 110 ng m^{-3} NH_4^+, yielding 0.5 $\mu g\ m^{-3}$ ammonium nitrate; the additional NO_3^-, 0.4 $\mu g\ m^{-3}$, is accounted as unbalanced nitrate. We have placed ammonium nitrate with the pollution component, and unbalanced NO_3^- with mineral dust: We thus assume that the ionic balance is provided by crustal elements, such as Ca [see, e.g., *Krueger et al.*, 2004]. We tend to believe that the unbalanced nitrate may be underestimated from our data set, due to the fact that ten samples, associated to significant dust advection episodes, were omitted in the IC analysis. If we could assume, for a crude evaluation, that unbalanced nitrate is proportional to Ca, we would increase its average concentration by 50% in order to account for the missing samples. A final observation on nitrate: In the polluted air mass, we have found a NO_3^-/SO_4^{2-} ratio of 0.1 (ratio of balanced NO_3^- to total SO_4^{2-} in both PM_{10} and PM_1 fractions). This is in line with the conclusions by *Henning et al.* [2003], i.e., that low values are found at remote sampling sites.

[33] The average aerosol concentration reconstructed by APCA amounts to 14.2 $\mu g\ m^{-3}$, 88% of the gravimetric determination. The reconstructed evolution with time of the three components is shown in Figure 2: As expected, the different aerosol types exhibit a quite different behavior, but the independent reconstructions by APCA and stoichiometric considerations are similar. In Figure 2b, only ammonium sulfate (deduced from elemental S) is displayed with the stoichiometric curve, since OM data are unavailable for PM_{10}: This is the reason for the strong quantitative difference between the two curves in Figure 2b. The PM_{10} pollution component is strongly correlated to gravimetric PM_1 (linear regression correlation coefficient 0.89, after reduction of the data set to a 48-hour resolution): This fact, in combination with the results for the compositional reconstruction of PM_1 in section 3.2 and to the factor loadings for aerosol sizes in Table 4 leads to the conclusion that PM_1 is mostly associated to the pollution component, and represents $\sim$70% of it (7.1 $\mu g\ m^{-3}$ out of 9.7).

[34] The presence of V among crustal elements deserves a comment, since this element is often associated with residual oil combustion [*Lee et al.*, 1999; *Li et al.*, 2004; *Almeida et al.*, 2005], and in Table 4 its factor loading (0.66) is much smaller than for other crustal elements ($\geq$0.95). In fact, V is

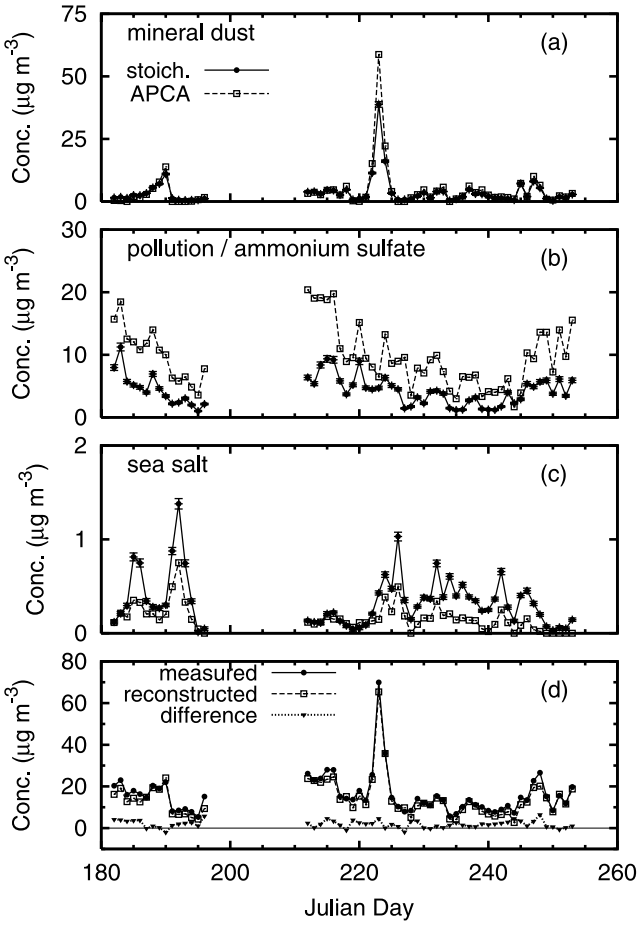

Figure 2. Concentration for the PM_{10} aerosol types identified during the Mount Cimone campaign, quantified by stoichiometric approach (solid circles, solid line) and by absolute principal component analysis (APCA) (open squares, dashed line): (a) mineral dust, (b) pollution (APCA) and ammonium sulfate (stoichiometric), and and (c) sea salt. (d) Comparison of gravimetric results (solid circles, solid line) and PM_{10} aerosols reconstructed by adding the three APCA components displayed in Figures 2a–2c (open squares, dashed line). Also shown is the difference between the two (solid triangles, dotted line).

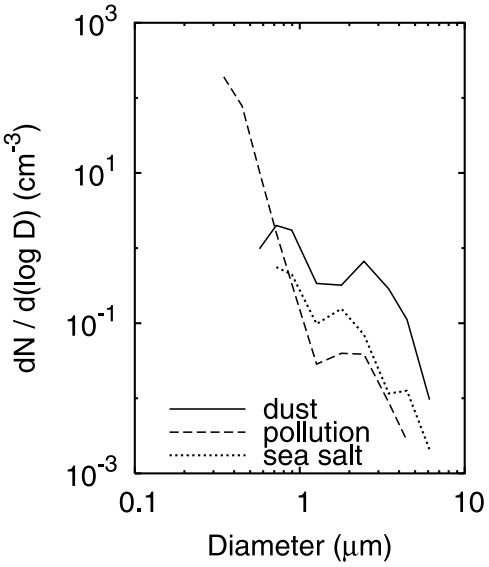

Figure 3. Number size distributions for mineral dust (solid line), pollution (dashed line), and sea salt (dotted line) at Mount Cimone during summer 2004, as deduced from the APCA.

present in a very small quantity (average 3.1 ng m^{-3} for PM_{10} samples above the minimum detection limit; concentration below the minimum detection limit, 1.5 ng m^{-3}, for 22 PM_{10} samples). However, it must be said that V events are seen in the data set: In some cases they occur on days characterized by preponderance of pollution, but on major mineral dust events a V signal is clearly seen. For instance on JD 223, 7.9 ng m^{-3} V are observed, with a Si/V ratio of 920, and on JD 190, 4.1 ng m^{-3} V are observed, with a Si/V ratio of 550; the Si/V ratios must be compared to the natural Si/V ratio in the Earth's crust, which is 2100 according to the concentrations reported by *Lide* [1992]. We believe that although the data are little above the minimum detection limit and this variable is not as robust as other concentrations, some signal of crustal V is actually seen on major mineral dust events, thanks to the distance from oil combustion sources.

[35] Figure 2d compares the aerosol reconstruction by APCA to the gravimetric determination, and displays the missing part ($\sim$2 μg m^{-3} on average). Results obtained with both approaches (multivariate and compositional) are in agreement (Table 5), taken into account that the methodologies are quite different. A reasonable quantitative estimate of the different contributors to the Mount Cimone PM_{10} (to the first significant digit) can be summarized as follows: 10 μg m^{-3} pollution, 4 μg m^{-3} mineral dust, and 0.2 μg m^{-3} sea salt. The proportions of ammonium sulfate and ammonium nitrate to the pollution component reflect those in total PM_1, and thus we can roughly estimate that this peculiarity may be extended to organic matter, for which we have no data in the PM_{10} fraction. With this assumption, OM could almost fill the gap between the APCA and stoichiometric approaches.

Table 6. Number Density, Effective Diameter, and Mode Diameters of the Size Distributions Displayed in Figure 3[a]

Component (APCA)	N, cm^{-3}	D_{eff}, μm	D_{mode}, μm
Mineral dust	1.7	2.7	0.7, 2.5
Pollution	75	0.44	$\leq$0.3, 2.2
Sea salt	0.33	2.3	$\leq$0.7, 1.8, 4.5

[a]The effective diameter is defined as the ratio of the third to the second moment of the size distribution.

Table 7. Source Apportionment for the Modena PM_{10} Aerosols, Derived From Elemental Concentrations and APCA[a]

		Average Concentration	
Component	Correlated Elements	Micrograms per Cubic Meter	Percentage
Mineral dust	Mg, Al, Si, K, Ca, Ti, Mn, Sr	10	28
Traffic	Cr, Mn, Fe, Cu, Zn, Pb	6	17
Sea salt	Na and Cl	1	3
Sulfates	S and Br	14	39
Reconstructed		31	86
Average PM_{10}		36	100

[a]The collection of samples in the town of Modena was carried out by the Regional Agency for Prevention and Environment, Emilia-Romagna.

3.4. Size Distributions

[36] As mentioned above, daily OPC size distributions have been included in the APCA. While at every moment the measured size distribution expresses a mix of the three components that have been identified, reflecting the fact that different air masses are more or less mixed, we can construct a per component size distribution by examining the source profiles determined with APCA. The obtained distributions are displayed in Figure 3, and their principal parameters are summarized in Table 6. It can be seen that the pollution component is dominated by a relatively large number of small particles, whereas the mineral dust and sea salt components are characterized by large particles in a relatively small abundance. The size distributions are bimodal, and the sea salt distribution is even trimodal, although this trimodality may not be considered fully significant.

3.5. Features of Modena Aerosols

[37] Results of PM_{10} sampling at Modena and elemental analysis thereof have been given elsewhere [*D'Alessandro et al.*, 2006], and are here briefly outlined since these data will be later used in comparison with the Mount Cimone data. The average PM_{10} concentration was 36 μg m^{-3} (standard deviation 12 μg m^{-3}). The combined use of the elemental concentrations determined by ED-XRF and of APCA permitted the identification of the four components listed in Table 7: We can see that the identified components are qualitatively similar with the Mount Cimone case, except for the presence of an additional "traffic" component.

3.6. Discussion

[38] Our results for PM_{10} can be compared to previous observations in the Mediterranean area. At Stelvio National Park, Italy (1300 m amsl), total suspended particulate (TSP) observations yielded 26.5 and 31.1 μg m^{-3} for summer and spring, respectively [*Braga Marcazzan et al.*, 1993]; a Saharan peak of 64.4 μg m^{-3} was also reported (26.0 μg m^{-3} of which are reconstructed as mineral dust using Particle Induced X-ray Emission, by taking oxides into account). When the S elemental concentration given in

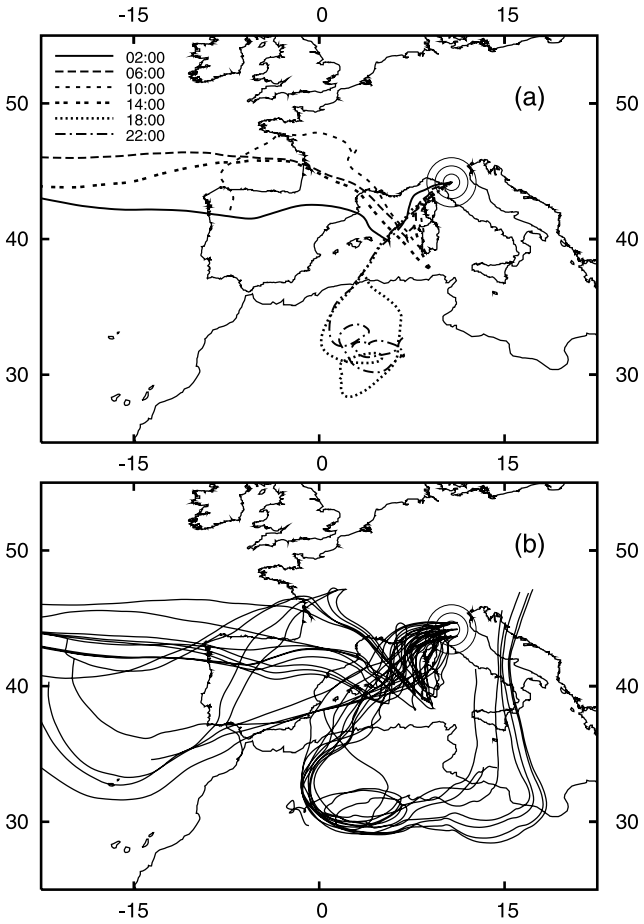

Figure 4. Trajectories ending at Mount Cimone on Julian day (JD) 223. The Mount Cimone site (44°11′N, 10°42′E, 2165 m above mean sea level) is at the center of the displayed target. (a) Back trajectories ending exactly at the Mount Cimone site at different times of day (local time). (b) Ensemble of 27 back trajectories ending around Mount Cimone at 0600 local time (see text). Trajectories have been computed with the Hybrid Single-Particle Lagrangian Integrated Trajectory (Hysplit) model, kindly provided by the NOAA Air Resources Laboratory.

this reference is converted to ammonium sulfate, 6 and 4 μg m^{-3} are found for summer and spring, respectively. At Jungfraujoch, Switzerland (3580 m amsl), however, the TSP level is much lower: The annual means range 3–5 μg m^{-3} and the average for Saharan dust events is 7.3 μg m^{-3} on 48-hour samples [*Collaud Coen et al.*, 2004]. An outstanding event at the same site reported a TSP concentration of 118 μg m^{-3} [*Schwikowski et al.*, 1995]. The ionic composition of the Jungfraujoch aerosols is given by *Henning et al.* [2003]: By converting their results for sulfate ions into ammonium sulfate mass concentration, 0.94 and 0.13 μg m^{-3} are found in summer and winter, respectively. Care is needed, however, when comparing PM_{10} and TSP concentrations, as their ratio depends on size distribution [see, e.g., *Querol et al.*, 2004]. The particulate matter concentrations at Stelvio National Park, Mount Cimone and Jungfraujoch show an inverse correlation with site altitude (as one would expect).

[39] Knowing that our measurements were taken at a site isolated from direct anthropogenic emissions, the concentrations obtained can be considered significant when compared to concentrations taken for reference at urban sites: In the European Union, for instance, a limit on average PM_{10} concentrations of 20 μg m^{-3} has been proposed for 2010, and it has been proposed that concentrations larger than 50 μg m^{-3} should not be tolerated for more than 7 days per year (indicative limit values for stage II, as in directive 1999/30/EC). We note, however, that our average of 16.1 μg m^{-3} cannot be assumed representative of the annual average at Mount Cimone, as our measurements refer to a relatively short period of time and to the summer season only. It must also not be assumed as representative of boundary layer PM concentration, since our measurements have been taken at an altitude of 2 km above sea level, and thus above the boundary layer for a significant fraction of observation time. It is anyways noteworthy that a single mineral dust episode was associated to a concentration of as much as 69.9 μg m^{-3}, and that episodes with even larger concentrations have been found frequent in the Mediterranean basin.

4. Transport Mechanisms

[40] In this section we wish to track the origin of the different air masses and try to find a hint on where the aerosols were originated and why they display the observed variability.

4.1. Mineral Dust

[41] In Figure 4a, six 3-D, 10-day, back trajectories ending at Mount Cimone at different times on JD 223 are displayed. The two evening back trajectories (1800 and 2200 local time) show air transport from the northern African continent: It seems therefore reasonable to conclude that the large mineral dust peak observed on JD 223 (PM_{10} concentration, 69.9 μg m^{-3}) is due to African air mass transport. Note that four of the displayed trajectories do not overpass Africa: Therefore, apparently, the Saharan dust event should not have been observed at Mount Cimone on the morning of JD 223. This is in contrast with our observations of the coarse particle number concentration (Figure 5), which suggest that the mineral dust event began around 1900 on JD 222, and ended around 0300 on JD 224. Therefore we need a more sophisticated approach than running isolated trajectories: According to *Stohl* [1998] a single trajectory is in general not sufficient for reliably describing the path of an air parcel. A problem originates from the amplification of small position disturbances in divergent wind flows [*Seibert*, 1993; *Baumann and Stohl*, 1997].

[42] We have chosen a method similar to the one proposed by *Collaud Coen et al.* [2004]: We run ensembles of 27 10-day back trajectories, with slightly differing endpoints. Endpoints are shifted by ±0.5° in latitude and longitude and by ±200 m in altitude (the horizontal shift being of the order of a third of the meteorological grid point separation). Figure 4b, for instance, displays the back trajectory ensemble with endpoint at 0600 local time on

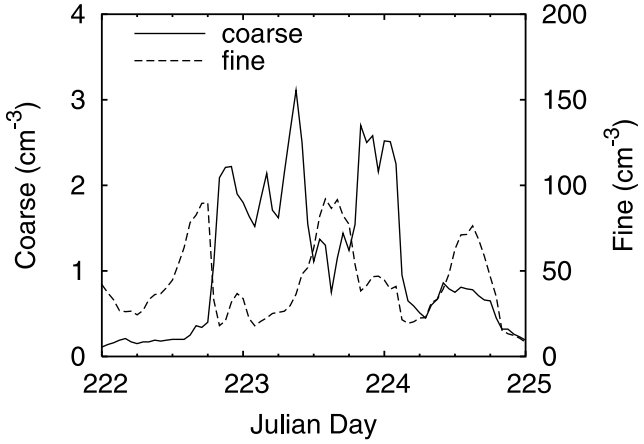

Figure 5. Coarse (solid line) and fine (dashed line) particle number concentration at Mount Cimone during and around the mineral dust event on JD 223.

JD 223: We can see that part of the trajectories overpass Africa, while another part do not. This picture is quite different than the one given by the 0600 trajectory on Figure 4a, which belongs to the trajectories that do not pass above the African continent.

[43] Trajectory ensembles allow to simply extract some statistical information, such as the portion of trajectories overpassing the African continent, the average number of days spent over Africa, and the overpassing altitude above the source region. Ensembles similar to the one displayed in Figure 4b have been run for the whole campaign period: Six ensembles per day have been run, spaced by 4-hour intervals. All runs belonging to one day (162 trajectories) have then been considered as a comprehensive ensemble, and daily statistics has been extracted. For instance, considering JD 223 as a whole, it results that 53% of the trajectories overpass Africa, and on average the time spent on that continent is 3.1 days. For 57% of their African time, JD 223 trajectories are found at an altitude smaller than 1500 m amsl, and for 96% at an altitude lower than 3500 m amsl.

[44] The average time spent over Africa has been retained as an indicator of the occurrence of African dust events, and has been plotted in both Figures 6a and 6b (open squares, dashed line). Note that 36% of the time spent over Africa corresponds to an altitude lower than 1500 m amsl, and 80% to an altitude lower than 3500 m amsl (whole campaign). In Figure 6, the Si concentration (Figure 6a) and the coarse particle number concentration (Figure 6b) have also been displayed. By visual comparison, it can be seen that this representation simply explains in terms of African air mass transport all significant dust peaks, as recognized by the increased concentration of Si and coarse particles. The picture provided by Figure 6 allows us to confidently conclude that dust variations at Mount Cimone during our summer campaign are explained by African dust transport.

4.2. Sea Salt

[45] The sea salt concentration exhibits sudden increases in concentration, in a similar way to mineral dust (Figure 2). A first glance at back trajectories run for sea salt episodes (not displayed here) shows that air masses may overpass both the Atlantic Ocean and the Mediterranean Sea, and that the time spent over the Atlantic can be much longer than the time spent over the Mediterranean; moreover the Atlantic part of the trajectories is often found at quite low altitudes (~1 km or less). It is therefore credible that mixing within the marine boundary layer over the Atlantic causes sea spray to enter the transported air mass arriving at Mount Cimone. The Mediterranean part of these trajectories, on the contrary, is rather short, and often found at more than 2 km above sea level. For these reasons, we think that marine aerosols found during our campaign are most probably originated above the Atlantic.

[46] However, processing trajectory ensembles systematically, in a way similar to what has been described for mineral dust (not shown here) does not yield conclusive information: As a matter of fact most trajectories spend a long time over the Atlantic, even for days when no signal of sea salt is measured at Mount Cimone. We conclude that the methodology used for identifying African dust events cannot be easily extended to other aerosol sources, and that a reasonable doubt on the origin of the salt remains. A possible explanation of this shortcoming is rainout along the transport path from the Atlantic to Mount Cimone, and we believe that an improved treatment of back trajectories for aerosol studies could take precipitation into account.

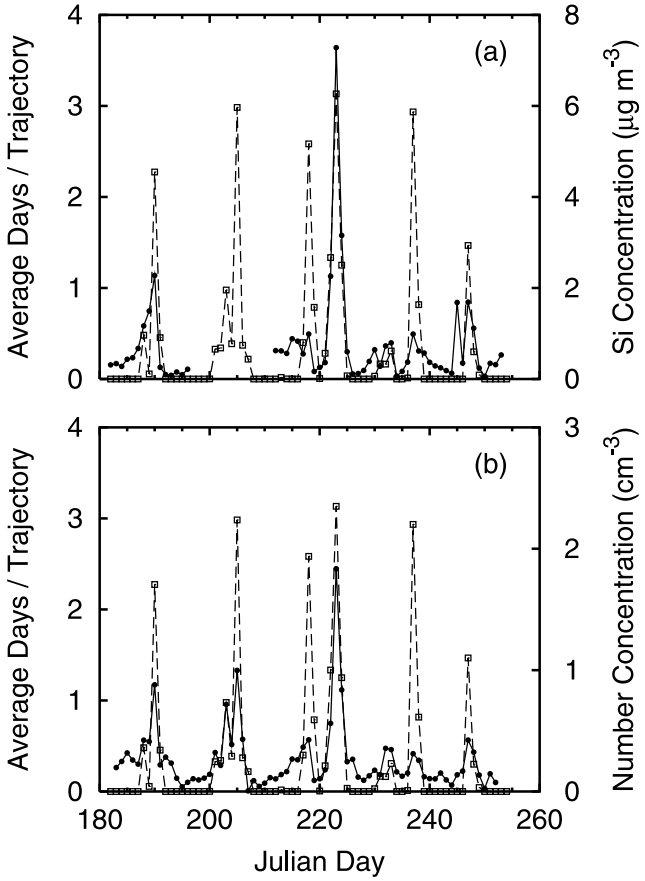

Figure 6. Average trajectory time over the African continent in days (open squares, dashed line), compared to (a) Si concentration (PM_{10}) and (b) coarse particle number concentration (solid circles, solid line).

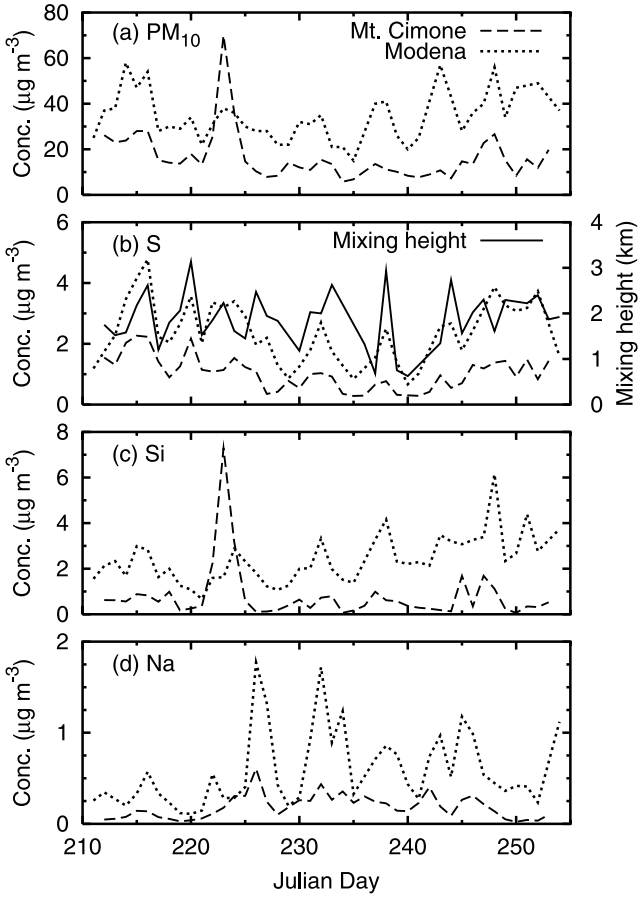

Figure 7. Concentrations of (a) PM_{10}, (b) S in PM_{10}, (c) Si in PM_{10}, and (d) Na in PM_{10} at Mount Cimone (dashed lines) and in Modena (dotted lines). In Figure 7b the mixing height at San Pietro Capofiume (altitude above mean sea level) is also displayed (solid line).

4.3. Pollution

[47] The concentration of pollution aerosols, well correlated with S, shows a rather different behavior than mineral dust and sea salt (Figure 2): Their concentration is dominant (60% of PM_{10}), but shows much less variability. According to APCA, for instance, this aerosol type accounts for 21% of the aerosol variance (Table 4). This low variance suggests a nearby source, less subject to the randomness of long-range transport, and the principal candidates are the Po Valley, one of the most industrialized regions in Europe, lying on the northeastern side of the Apennines, and the valleys of Tuscany on the southern side. In Figure 7b, S concentrations at Modena and Mount Cimone are compared for the common part of the data set: Despite being much lower than S concentrations at Modena (less than a half), S concentrations at Mount Cimone show a similar behavior (linear regression correlation coefficient: 0.78), thus confirming our hypothesis.

[48] In the case of regional-scale tracer dispersion, the meteorological mechanism is quite different than the long-range transport by synoptic winds examined earlier, and might be better related to convective motion and vertical mixing within the Planetary Boundary Layer, where an air parcel quickly looses its identity. Local meteorological effects also play a role, as mountain sites are often influenced by anabatic and katabatic winds during summer [*Zaveri et al.*, 1995]. A hint of the effect of vertical mixing is given for instance in the plot of fine particles in Figure 5, where a daily maximum around 1500 local time is clearly seen. This is confirmed by the average summertime diurnal trend for fine particles, which exhibits lowest concentrations at nighttime and an increase in the afternoon (1500–1800 local time). A similar diurnal cycle for Mount Cimone has already been described by *Fischer et al.* [2003] and *Van Dingenen et al.* [2005].

[49] The analysis of mixing height can provide useful information for describing the transport processes related with the presence of regional pollution at Mount Cimone. The daily mixing height determined from radiosonde data is displayed in Figure 7b, together with the two S concentrations: The correlation appears convincing. In particular, some of the highest S loadings at Mount Cimone have been recorded simultaneously with high S concentrations in Modena, and large mixed layer depths in the Po basin. We conclude that the transport of regional aerosol under favorable meteorological conditions represents one of the most important sources of pollution at Mount Cimone during our summer campaign.

4.4. Relationship With Po Valley Aerosols

[50] In Figure 7b, S concentrations for PM_{10} at Modena and Mount Cimone have been related. In this section we shall investigate whether this behavior can be extended to other concentrations, representative of different aerosol types. Beside the S concentration, Figure 7 displays the variations of PM_{10}, Si and Na at both sites; Si and Na concentrations being considered representative of the mineral dust and sea salt components of the aerosol, respectively. Looking at PM_{10} (Figure 7a), one notices that some features are indeed common to both sites, but that in general the correlation of the two sequences is rather weak (linear regression correlation coefficient: 0.31; increased to 0.53 by removing the outliers on JD 222–224).

[51] In particular, note that the largest concentration occurring at Mount Cimone (JD 223) is associated to an "average" concentration in Modena, although the presence of a relative maximum may lead the observer to believe that the dust event was observed in Modena as well. Nevertheless, a larger concentration of S (3.2 $\mu g\ m^{-3}$, Figure 7b), as compared to Si (1.6 $\mu g\ m^{-3}$, Figure 7c) suggests that this maximum must not be ascribed to an increase of mineral dust alone. Note, however, that a weak Si maximum is observed in Modena on JD 224 (2.9 $\mu g\ m^{-3}$). In general, the correlation between the two Si concentrations in Figure 7c seems even weaker than for PM_{10} (linear regression correlation coefficient: 0.03; increased to 0.43 by removing the outliers on JD 222–224). This decorrelation can be in part explained by the fact that Si events at Modena occur sometimes one day earlier (JD 233) or later (JD 223, 237, 247) than Si events at Mount Cimone, as already pointed out by *Bonasoni et al.* [2004] for urban areas in the Po basin.

[52] As for what Na is concerned (Figure 7d), the correlation at the two sites is rather good (linear regression correlation coefficient: 0.76), suggesting that marine advec-

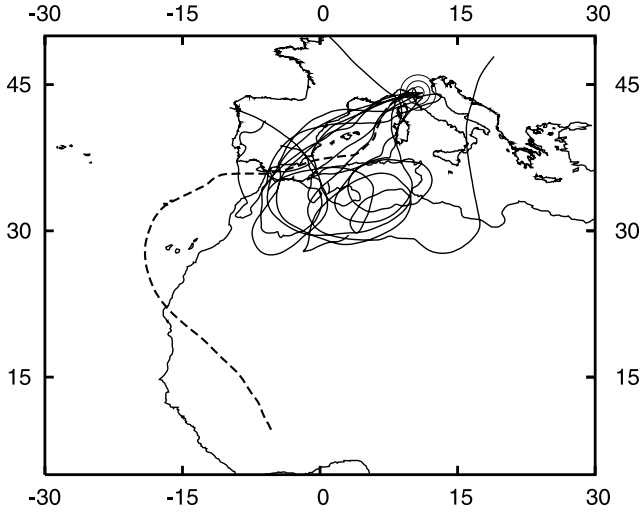

Figure 8. Individual back trajectories for days classified for Saharan dust transport to Mount Cimone (see text). For each of the following days, one daily trajectory has been randomly selected from the ensemble: JD 190, 203, 205, 218, 219, 222, 223, 224, 237, 238, and 247. The trajectory for JD 247 is plotted with a dashed line. Trajectories have been computed with the Hysplit model, kindly provided by the NOAA Air Resources Laboratory.

tion events at both sites tend to occur simultaneously. Only for dust events, therefore the two sites seem decorrelated. This circumstance suggests that the advection of dust at Mount Cimone takes place during free tropospheric conditions (see also the noontime relative minimum in the coarse particle number in Figure 5).

5. African Dust and Geochemical Signatures

[53] In Figure 8, individual back trajectories for days affected by African dust transport to Mount Cimone are plotted. Days have been selected according to the criterion that the average time over Africa per trajectory (Figure 6) is at least 0.5 day. For each selected day, one of the computed trajectories within the ensemble has been randomly chosen. Figure 8 gives an idea of where in Africa the dust is originated. Most of the trajectories, in fact, overpass the northwestern part of the continent (Morocco, northern Algeria and Tunisia): The observed dust episodes for those days are therefore attributed to the northern Sahara. However, a special attention is deserved by the episode which occurred on JD 247 (broken line), since the plotted trajectory originates in the Sahelian region (Mali and Mauritania). The ensemble computed for this day is coherent with the randomly chosen trajectory.

[54] Elemental ratios are often used as geochemical fingerprints of African dust [see, e.g. *Martin et al.*, 1990; *Perry et al.*, 1997; *Chiapello et al.*, 1997; *Formenti et al.*, 2001; *Borbély-Kiss et al.*, 2004]. In Figure 9, a few of these ratios have been depicted, distinguishing between northern Saharan episodes, the Sahelian episode, and all the other campaign days. These plots have to be compared to those presented by *Chiapello et al.* [1997] and *Borbély-Kiss et al.* [2004].

[55] In Figures 9a and 9b, points corresponding to northern Saharan events are in a region of the plot which corresponds to the graphs displayed in the work of *Chiapello et al.* [1997] for northwestern Sahara. In Figure 9c, points corresponding to northern Saharan events are slightly higher in the plot than the Saharan points displayed in the work of *Borbély-Kiss et al.* [2004]: Our data set tends to exhibit larger Ti/Fe and Ti/Ca ratios. In Figures 9a–9c, the Sahelian event of JD 247 shows elemental ratios more or less in the average of the northern Saharan events: This observation is in contrast with the conclusions of other authors, as, for instance, *Chiapello et al.* [1997], but has to be considered with care since it represents only one observation day. Ratios for the remaining campaign days display some overlap with the African dust events, but on average exhibit a different behavior. According to our limited data set, the ratios which

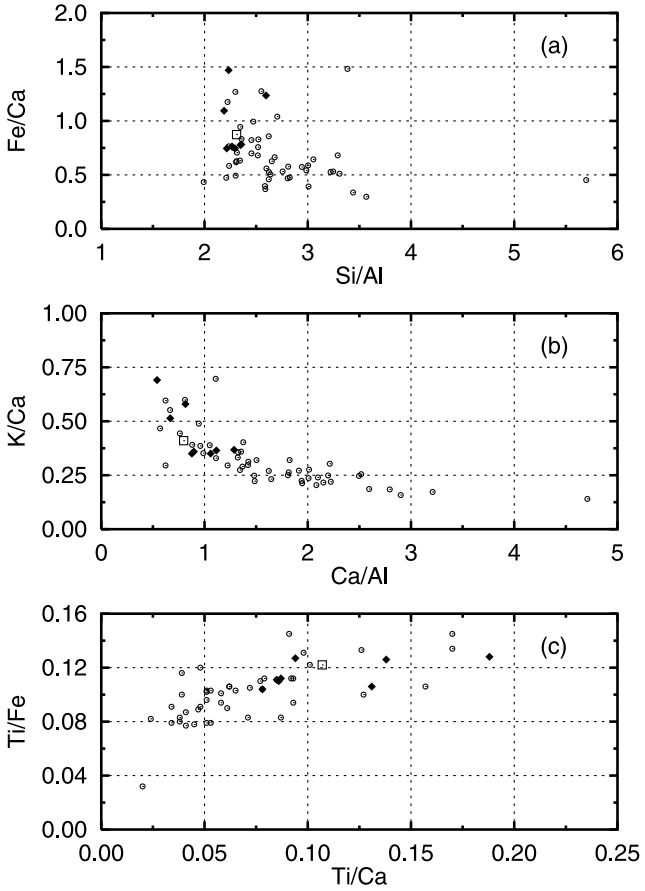

Figure 9. Elemental ratios of crustal elements, computed for the Mount Cimone PM_{10} daily samples: (a) Fe/Ca and Si/Al, (b) K/Ca and Ca/Al, and (c) Ti/Fe and Ti/Ca. Solid diamonds indicate days for which back trajectories indicate transport from the northern Sahara. Open squares indicate JD 247 for which back trajectories indicate transport from the Sahel region. Open circles denote all the other days for which the average trajectory time over Africa (Figure 6) is smaller than 0.5 day.

Table 8. Average Elemental Ratios Computed From the Mount Cimone PM_{10} Samples for Days Characterized by Transport From the African Continent and for the Other Days[a]

Ratio	Days of African Transport	Other Days
Si/Al	2.31 ± 0.12	2.73 ± 0.58
Fe/Ca	0.94 ± 0.26	0.67 ± 0.26
Ca/Al	0.90 ± 0.23	1.68 ± 0.78
K/Ca	0.44 ± 0.12	0.31 ± 0.12
Ti/Ca	0.110 ± 0.036	0.070 ± 0.036
Ti/Fe	0.116 ± 0.009	0.100 ± 0.021

[a]Average and standard deviation are given.

appear more effective in distinguishing African dust events are Si/Al, Ca/Al, Ti/Ca and Ti/Fe.

[56] Average elemental ratios are given in Table 8. Si/Al, Fe/Ca and K/Ca ratios for the African case match almost identically the ratios derived by *Chiapello et al.* [1997] at Cape Verde for the northwestern Saharan sector. A difference arises in the Ca/Al ratio, which is larger in our data set by 50% (but still compatible within the standard deviation). A difference arises also with the data by *Borbély-Kiss et al.* [2004] for the Saharan Ti/Ca and Ti/Fe ratios, which are exceeded in the present work by 40–50%. Finally, ratios derived at Mount Cimone are somewhat different than ratios calculated from the concentration data for sand samples in the Saharan region given by *Krueger et al.* [2004]. It must be pointed out, however, that the sampling site used in that research was located in the Central Sahara, at a large distance from the territories of the northern Sahara which are, according to back trajectories, the main source of dust at Mount Cimone.

6. Conclusions

[57] Daily aerosol properties have been measured at Mount Cimone during a 3-month period in summer 2004. On average, 16.1 μg m^{-3} have been observed (PM_{10}), but a large variability of all measured parameters dominated the campaign, as is usual with aerosol measurements. A combination of source apportionment approaches using stoichiometric considerations and multivariate statistics allowed us to separate the signal due to three different aerosol classes, each being driven by an independent variability pattern: mineral dust, anthropogenic pollution, and sea salt.

[58] The most abundant component of the aerosol has been associated to anthropogenic pollution (10 μg m^{-3}, mostly in the fine fraction); this component has also been found to yield a relatively small contribution (21%) to the overall aerosol variability. Regarding the composition of pollution, the representation is more complete with the PM_1 fraction, for which carbonaceous concentrations are available. The most of it is represented by ammonium sulfate and organic matter, in a nearly 1:1 proportion, which together represent the 86% of the total and show a significant correlation with each other. Small concentrations of ammonium nitrate, elemental carbon, and crustal oxides were also identified. A small nitrate/sulfate ratio has been found, as already observed by *Henning et al.* [2003] at the Jungfraujoch. Simultaneous observations in Modena and the mixed layer depth suggested that for a large part this component could be ascribed to regional pollution, transported at Mount Cimone under a boundary layer convection regime.

[59] Mineral dust reconstruction by APCA was found quantitatively compatible with a composition based on the metallic oxides that are found in the Earth's crust, amounting to 4 μg m^{-3}. Besides crustal oxides, ~10% of the mineral dust concentration has been attributed to nitrate ions. The presence of nitrate in advected mineral dust particles confirms the conclusions of *Henning et al.* [2003], *Putaud et al.* [2004] and *Krueger et al.* [2004]. Mineral dust contributed mostly to the concentration of coarse particles. Despite representing on average only one fourth of the aerosol concentration, it has been the cause for most (56%) of the observed aerosol variability. By tracing this variability with ensembles of back trajectories computed with the Hysplit model, we could explain this aerosol class in terms of long-range transport from the African continent, particularly from the northern Sahara. Elemental signatures for dust events, often used as geochemical tracers, have been found to correspond to the results of *Chiapello et al.* [1997] in what Si/Al, Fe/Ca and K/Ca are concerned. Ratios for Ca/Al, Ti/Ca and Ti/Fe showed a 40–50% exceedance with respect to published results by *Chiapello et al.* [1997] and *Borbély-Kiss et al.* [2004]. In one case trajectories displayed dust advection from the Sahel.

[60] The observed concentration of sea salt at Mount Cimone was quite low (average 0.2 μg m^{-3}, maximum 1–1.5 μg m^{-3}). Roughly speaking, the concentration of sea salt has been associated to low aerosol periods and to the "cleaning" of the atmosphere after African dust events.

[61] The three aerosol classes explain 88% of the observed aerosol concentration and 84% of its variability. We have therefore provided an estimate, at this site and for the period of time under study, of the relative contribution of anthropogenic (pollution) and natural aerosol components (mineral dust and sea salt).

[62] **Acknowledgments.** This work has been supported by the Italian Ministry for Research (project MIUR-COFIN2003) and by Istituto Nazionale di Fisica Nucleare (INFN). The authors gratefully acknowledge the Italian Air Force Meteorological Service for providing access to the Mount Cimone site. Thanks are due to the NOAA Air Resources Laboratory for the provision of the Hysplit transport and dispersion model. Thanks are also due to the Regional Agency for Prevention and Environment, Emilia-Romagna, for the provision of PM_{10} samples collected in Modena.

References

Almeida, S. M., C. A. Pio, M. C. Freitas, M. A. Reis, and M. A. Trancoso (2005), Source apportionment of fine and coarse particulate matter in a sub-urban area at the western European coast, *Atmos. Environ.*, *39*, 3127–3138.

Baumann, K., and A. Stohl (1997), Validation of a long-range trajectory model using gas balloon tracks from the Gordon Bennett Cup 95, *J. Appl. Meteorol.*, *36*, 711–720.

Birch, M. E., and R. A. Cary (1996), Elemental carbon-based method for monitoring occupational exposures to particulate diesel exhaust, *Aerosol Sci. Technol.*, *25*, 221–241.

Bonasoni, P., and P. Cristofanelli (2001), Analysis of polluted ozone in a mountain area, in *Air Pollution IX*, edited by G. Latini, and C. A. Brebbia, pp. 579–585, WIT Press, Southampton, U. K.

Bonasoni, P., F. Evangelisti, U. Bonafè, F. Ravegnani, F. Calzolari, A. Stohl, L. Tositti, O. Tubertini, and T. Colombo (2000a), Stratospheric ozone intrusion episodes recorded at Mt. Cimone during the VOTALP project: Case studies, *Atmos. Environ.*, *34*, 1355–1365.

Bonasoni, P., A. Stohl, P. Cristofanelli, F. Calzolari, T. Colombo, and F. Evangelisti (2000b), Background ozone variations at Mt. Cimone station, *Atmos. Environ.*, *34*, 5183–5189.

Bonasoni, P., P. Cristofanelli, F. Calzolari, U. Bonafé, F. Evangelisti, A. Stohl, S. Zauli Sajani, R. Van Dingenen, T. Colombo, and Y. Balkanski (2004), Aerosol-ozone correlations during dust transport episodes, *Atmos. Chem. Phys.*, *4*, 1201–1215.

Borbély-Kiss, I., Á. Z. Kiss, E. Koltay, G. Szabó, and L. Bozó (2004), Saharan dust episodes in Hungarian aerosol: Elemental signatures and transport trajectories, *J. Aerosol Sci.*, *35*, 1205–1224.

Braga Marcazzan, G. M., P. Bonelli, E. Della Bella, A. Fumagalli, R. Ricci, and U. Pellegrini (1993), Study of regional and long-range transport in an Alpine station by PIXE analysis of aerosol particles, *Nucl. Instrum. Methods Phys. Res., Sect. B*, *75*, 312–316.

Chiapello, I., G. Bergametti, B. Chatenet, P. Bousquet, F. Dulac, and E. Santos Soares (1997), Origins of African dust transported over the northeastern tropical Atlantic, *J. Geophys. Res.*, *102*, 13,701–13,709.

Chiapello, I., J. M. Prospero, J. R. Herman, and N. C. Hsu (1999), Detection of mineral dust over the North Atlantic Ocean and Africa with the Nimbus 7 TOMS, *J. Geophys. Res.*, *104*, 9277–9291.

Chow, J. C., and J. G. Watson (1999), Ion chromatography in elemental analysis of airborne particles, in *Elemental Analysis of Airborne Particles*, vol. 1, edited by S. Landsberger, and M. Creatchman, pp. 97–137, Gordon and Breach, New York.

Chow, J. C., J. G. Watson, D. Crow, D. H. Lowenthal, and T. Merrifield (2001), Comparison of IMPROVE and NIOSH carbon measurements, *Aerosol Sci. Technol.*, *34*, 23–34.

Collaud Coen, M., E. Weingartner, D. Schaub, C. Hueglin, C. Corrigan, S. Henning, M. Schwikowski, and U. Baltensperger (2004), Saharan dust events at the Jungfraujoch: Detection by wavelength dependence of the single scattering albedo and first climatology analysis, *Atmos. Chem. Phys.*, *4*, 2465–2480.

Cristofanelli, P., P. Bonasoni, L. Tositti, U. Bonafè, F. Calzolari, F. Evangelisti, S. Sandrini, and A. Stohl (2006), A 6-year analysis of stratospheric intrusions and their influence on ozone at Mt. Cimone (2165 m above sea level), *J. Geophys. Res.*, *111*, D03306, doi:10.1029/2005JD006553.

D'Alessandro, A., F. Lucarelli, P. A. Mandò, G. Marcazzan, S. Nava, P. Prati, G. Valli, R. Vecchi, and A. Zucchiatti (2003), Hourly elemental composition and sources identification of fine and coarse PM10 particulate matter in four Italian towns, *J. Aerosol Sci.*, *34*, 243–259.

D'Alessandro, A., F. Marenco, F. Mazzei, S. Nava, P. Prati, and R. Vecchi (2006), Particolato Atmosferico a Modena nell'Estate 2004: Risultati dell'Analisi Elementale e Statistica, *Rep. INFN/TC-06/01*, Ist. Naz. di Fis. Nucl., Frascati, Italy.

Eldred, R. A., T. A. Cahill, and P. T. Feeney (1987), Particulate monitoring at US national parks using PIXE, *Nucl. Instrum. Methods Phys. Res., Sect. B*, *22*, 289–295.

El-Zanan, H. S., D. H. Lowenthal, B. Zielinska, J. C. Chow, and N. Kumar (2005), Determination of the aerosol mass to organic carbon ratio in IMPROVE samples, *Chemosphere*, *60*, 485–496.

Fischer, H., et al. (2003), Ozone production and trace gas correlations during the June 2000 MINATROC intensive measurement campaign at Mt. Cimone, *Atmos. Chem. Phys.*, *3*, 725–738.

Formenti, P., M. O. Andreae, L. Lange, G. Roberts, J. Cafmeyer, I. Rajta, W. Maenhaut, B. N. Holben, P. Artaxo, and J. Lelieveld (2001), Saharan dust in Brazil and Suriname during the Large-Scale Biosphere-Atmosphere Experiment in Amazonia (LBA)—Cooperative LBA Regional Experiment (CLAIRE) in March 1998, *J. Geophys. Res.*, *106*, 14,919–14,934.

Gobbi, G. P., F. Barnaba, R. Giorgi, and A. Santacasa (2000), Altitude-resolved properties of a Saharan dust event over the Mediterranean, *Atmos. Environ.*, *34*, 5119–5127.

Hansson, H.-C., B. G. Martinsson, and H. O. Lannefors (1984), Long range aerosol transport in southern Sweeden: An example of multivariate statistical evaluation methodology, *Nucl. Instrum. Methods Phys. Res., Sect. B*, *3*, 483–488.

Henning, S., E. Weingartner, M. Schwikowski, H. W. Gäggeler, R. Gehrig, K.-P. Hinz, A. Trimborn, B. Spengler, and U. Baltensperger (2003), Seasonal variation of water-soluble ions of the aerosol at the high-alpine site Jungfraujoch (3580 m asl), *J. Geophys. Res.*, *108*(D1), 4030, doi:10.1029/2002JD002439.

Intergovernmental Panel on Climate Change, (2001), *Climate Change 2001: The Scientific Basis*, edited by J. T. Houghton, et al., Cambridge Univ. Press, New York.

Keiding, K., J. F. Palmgren, and M. Z. Heidam (1986), Absolute modelling of urban aerosol elemental composition by factor analysis, *Anal. Chim. Acta*, *181*, 79–85.

Krueger, B. J., V. H. Grassian, J. P. Cowin, and A. Laskin (2004), Heterogeneous chemistry of individual mineral dust particles from different dust source regions: The importance of particle mineralogy, *Atmos. Environ.*, *38*, 6253–6261.

Lee, E., C. K. Chan, and P. Paatero (1999), Application of positive matrix factorization in source apportionment of particulate pollutants in Hong Kong, *Atmos. Environ.*, *33*, 3201–3212.

Li, Z., P. K. Hopke, L. Husain, S. Qureshi, V. A. Dutkiewicz, J. J. Schwab, F. Drewnick, and K. L. Demerjian (2004), Sources of fine particle composition in New York city, *Atmos. Environ.*, *38*, 6521–6529.

Lide, D. R. (Ed.) (1992), *CRC Handbook of Chemistry and Physics 1991–1992*, CRC Press, Boca Raton, Fla.

Malm, W. C., J. F. Sisler, D. Huffman, R. A. Eldred, and T. A. Cahill (1994), Spatial and seasonal trends in particle concentration and optical extinction in the United States, *J. Geophys. Res.*, *99*, 1347–1370.

Marcazzan, G. M., S. Vaccaro, G. Valli, and R. Vecchi (2001), Characterization of PM10 and PM2.5 particulate matter in the ambient air of Milan (Italy), *Atmos. Environ.*, *35*, 4639–4650.

Marcazzan, G. M., M. Ceriani, G. Valli, and R. Vecchi (2003), Source apportionment of PM10 and PM2.5 in Milan (Italy) using receptor modelling, *Sci. Total Environ.*, *317*, 137–147.

Martin, D., G. Bergametti, and B. Strauss (1990), On the use of the synoptic vertical velocity in trajectory model: Validation by geochemical tracers, *Atmos. Environ., Part A*, *24*, 2059–2069.

Mather, P. M. (1976), *Computational Methods of Multivariate Analysis in Physical Geography*, John Wiley, Hoboken, N. J.

Morales, C. (1986), The airborne transport of Saharan dust: A review, *Clim. Change*, *9*, 219–241.

Perry, K. D., T. A. Cahill, R. A. Eldred, D. D. Dutcher, and T. E. Gill (1997), Long-range transport of North African dust to the eastern United States, *J. Geophys. Res.*, *102*, 11,225–11,238.

Putaud, J.-P., R. Van Dingenen, A. Dell'Acqua, F. Raes, E. Matta, S. Decesari, M.C. Facchini, and S. Fuzzi (2004), Size-segregated aerosol mass closure and chemical composition in Monte Cimone (I) during MINATROC, *Atmos. Chem. Phys.*, *4*, 889–902.

Querol, X., A. Alastuey, S. Rodriguez, F. Plana, C. R. Ruiz, N. Cots, G. Massagué, and O. Puig (2001), PM10 and PM2.5 source apportionment in the Barcelona Metropolitan area, Catalonia, Spain, *Atmos. Environ.*, *35*, 6407–6419.

Querol, X., et al. (2004), Levels of particulate matter in rural, urban and industrial sites in Spain, *Sci. Total Environ.*, *334–335*, 359–376.

Rodríguez, S., X. Querol, A. Alastuey, G. Kallos, and O. Kakaliagou (2001), Saharan dust contributions to PM10 and TSP levels in southern and eastern Spain, *Atmos. Environ.*, *35*, 2433–2447.

Schwikowski, M., P. Seibert, U. Baltensperger, and H. W. Gäggeler (1995), A study of an outstanding Saharan dust event at the high-alpine site Jungfraujoch, Switzerland, *Atmos. Environ.*, *29*, 1829–1842.

Seibert, P. (1993), Convergence and accuracy of numerical methods for trajectory calculations, *J. Appl. Meteorol.*, *32*, 558–566.

Seibert, P., H. Feldmann, B. Neininger, M. Bäumle, and T. Trickl (2000), South foehn and ozone in the Eastern Alps—Case study and climatological aspects, *Atmos. Environ.*, *34*, 1379–1394.

Seinfeld, J. H., and S. N. Pandis (1998), *Atmospheric Chemistry and Physics—From Air Pollution to Climate Change*, John Wiley, Hoboken, N. J.

Stohl, A. (1998), Computation, accuracy and applications of trajectories—A review and bibliography, *Atmos. Environ.*, *32*, 947–966.

Streit, N., E. Weingartner, C. Zellweger, M. Schwikowski, H. W. Gäggeler, and U. Baltensperger (2000), Characterization of size-fractionated aerosol from the Jungfraujoch (3580 m asl) using total reflection X-ray fluorescence (TXRF), *Int. J. Environ. Anal. Chem.*, *76*, 1–16.

Swietlicki, E., H.-C. Hansson, and B. G. Martinsson (1987), PIXE elemental characterization of air masses using a multivariate statistical technique, *Nucl. Instrum. Methods Phys. Res., Sect. B*, *22*, 264–269.

Swietlicki, E., S. Puri, and H. C. Hansson (1996), Urban air pollution source apportionment using a combination of aerosol and gas monitoring techniques, *Atmos. Environ.*, *30*, 2795–2809.

Tegen, I., and I. Fung (1995), Contribution to the atmospheric mineral aerosol load from land surface modification, *J. Geophys. Res.*, *100*, 18,707–18,726.

Thurston, G. D., and J. D. Spengler (1985), A quantitative assessment of source contributions to inhalable particulate matter pollution in metropolitan Boston, *Atmos. Environ.*, *19*, 9–25.

Turpin, B. J., and H.-J. Lim (2001), Species contributions to PM2.5 mass concentrations: Revisiting common assumptions for estimating organic mass, *Aerosol Sci. Technol.*, *35*, 602–610.

Van Dingenen, R., J.-P. Putaud, F. Martins-Dos Santos, and F. Raes (2005), Physical aerosol properties and their relation to air mass origin at Monte Cimone (Italy) during the first MINATROC campaign, *Atmos. Chem. Phys. Discuss.*, *5*, 1067–1114.

Van Grieken, R., and A. A. Markowicz (1993), *Handbook of X-Ray Spectrometry*, CRC Press, Boca Raton, Fla.

Virkkula, A., M. Aurela, R. Hillamo, T. Mäkelä, T. Pakkanen, V.-M. Kerminen, W. Maenhaut, F. François, and J. Cafmeyer (1999), Chemical composition of atmospheric aerosol in European subartic: Contribution of

the Kola Peninsula smelter areas, central Europe, and the Arctic Ocean, *J. Geophys. Res.*, *104*, 23,681–23,696.

Zaveri, R. A., R. D. Saylor, L. K. Peters, R. McNider, and A. Song (1995), A model investigation of summertime diurnal ozone behaviour in rural mountainous locations, *Atmos. Environ.*, *29*, 1043–1065.

P. Bonasoni, F. Calzolari, and P. Cristofanelli, Institute of Atmospheric Sciences and Climate, National Research Council, Via Gobetti 101, Bologna I-40129, Italy.

M. Ceriani, G. Valli, and R. Vecchi, General Applied Physics Institute, University of Milan, Via Celoria 16, Milan I-20133, Italy.

M. Chiari, F. Lucarelli, and S. Nava, Physics Department, University of Florence, Via Sansone 1, Sesto Fiorentino (FI) I-50019, Italy.

A. D'Alessandro, F. Marenco, F. Mazzei, and P. Prati, Physics Department, University of Genoa, Via Dodecaneso 33, Genova I-16146, Italy. (tel: +39-091-7824133)

P. Fermo and A. Piazzalunga, Inorganic, Metallorganic and Analytical Chemistry Department, University of Milan, Via Venezian 21, Milan I-20133, Italy.